Articles

Catalytic Mechanism of Glycine *N*-Methyltransferase[†,▽]

Yoshimi Takata,[‡,§,||] Yafei Huang,[‡,||,⊥] Junichi Komoto,[‡] Taro Yamada,[‡] Kiyoshi Konishi,[§,#] Hirofumi Ogawa,[§] Tomoharu Gomi,[§] Motoji Fujioka,[§] and Fusao Takusagawa*[,‡]

Department of Molecular Biosciences, University of Kansas, 1200 Sunnyside Avenue, Lawrence, Kansas 66045-7534, and Department of Biochemistry, Faculty of Medicine, Toyama Medical and Pharmaceutical University, Sugitani, Toyama 930-0194, Japan

Received February 12, 2003; Revised Manuscript Received May 22, 2003

ABSTRACT: Methyltransfer reactions are some of the most important reactions in biological systems. Glycine *N*-methyltransferase (GNMT) catalyzes the *S*-adenosyl-L-methionine- (SAM-) dependent methylation of glycine to form sarcosine. Unlike most SAM-dependent methyltransferases, GNMT has a relatively high K_M^{SAM} value and is weakly inhibited by the product *S*-adenosyl-L-homocysteine (SAH). The major role of GNMT is believed to be the regulation of the cellular SAM/SAH ratio, which is thought to play a key role in SAM-dependent methyltransfer reactions. Crystal structures of GNMT complexed with SAM and acetate (a potent competitive inhibitor of Gly) and the R175K mutated enzyme complexed with SAM were determined at 2.8 and 3.0 Å resolutions, respectively. With these crystal structures and the previously determined structures of substrate-free enzyme, a catalytic mechanism has been proposed. Structural changes occur in the transitions from the substrate-free to the binary complex and from the binary to the ternary complex. In the ternary complex stage, an α-helix in the N-terminus undergoes a major conformational change. As a result, the bound SAM is firmly connected to protein and a "Gly pocket" is created near the bound SAM. The second substrate Gly binds to Arg175 and is brought into the Gly pocket. Five hydrogen bonds connect the Gly in the proximity of the bound SAM and orient the lone pair orbital on the amino nitrogen (N) of Gly toward the donor methyl group (C_E) of SAM. Thermal motion of the enzyme leads to a collision of the N and C_E so that a S_N2 methyltransfer reaction occurs. The proposed mechanism is supported by mutagenesis studies.

Glycine *N*-methyltransferase [*S*-adenosyl-L-methionine (SAM):glycine methyltransferase, EC 2.1.1.20; GNMT] catalyzes the SAM[1]-dependent methylation of Gly to form sarcosine (*1*). Blumenstein and Williams first reported that GNMT activity is high in liver supernatants from guinea pig, rat, rabbit, and mouse and relatively low in analogous preparations from calf, pig, lamb, and chicken livers (*1*). Later, Ogawa et al. showed that human, rat, and rabbit livers contain relatively large amounts of GNMT (0.1−3% of the total soluble protein) (*2*). GNMT has also been found in the nucleus of liver cells (*3*). The distribution of GNMT in a variety of rat tissues was examined immunohistochemically (*4*). In liver, GNMT was most abundant in the periportal region, whereas in kidney it was seen primarily in the proximal convoluted tubules. In pancreas, GNMT was abundant, principally in the exocrine tissue. GNMT was present in the striated duct cells of the submaxillary gland. In the jejunum, GNMT was found in the epithelial cells of the villi.

SAM-dependent methyltransferases are generally strongly inhibited by the product *S*-adenosyl-L-homocysteine (SAH), and the cellular SAM/SAH ratio is thought to play a key role in methyltransfer reactions (*5*, *6*). GNMT is a good candidate for a regulator of the SAM/SAH ratio for the following reasons. The enzyme is abundant in liver and the product sarcosine has no known physiological role and is converted back to Gly by sarcosine dehydrogenase (*7*). The K_i values of GNMTs for SAH are in the range of 35−80 μM and are much higher than the values of other methyl-

[†] The work carried out at the University of Kansas was supported by NIH Grant GM37233.

[▽] The atomic coordinates of GNMT:(SAM + acetate) and R175K:SAM have been deposited with the Protein Data Bank (PDB ID 1NBH and 1NBI).

* To whom correspondence should be addressed. Tel: (785) 864-4727. Fax: (785) 864-5321. E-mail: xraymain@ku.edu.

[‡] University of Kansas.

[§] Toyama Medical and Pharmaceutical University.

[||] Y.T. and Y.H. contributed equally to this work.

[⊥] Present address: Skirball Institute of Molecular Medicine, New York University, New York, NY 10016.

[#] Present address: Department of Microbiology, The Nippon Dental University, 1-9-20 Fujimi, Chiyoda-ku, Tokyo 102, Japan.

[1] Abbreviations: GNMT, rat liver glycine *N*-methyltransferase; R175K, Y21F, Y33F, Y194F, Y220F, and Y242F, mutated GNMTs; SAM, *S*-adenosyl-L-methionine; SAH, *S*-adenosyl-L-homocysteine; GNMT:(SAM + acetate), SAM- and acetate-bound GNMT; R175K:SAM, SAM-bound R175K; R175K:SAH, SAH-bound R175K; WT, wild-type GNMT; helix A, slightly irregular helix composed of amino acid residues 25−54; Y194 loop, loop between α7 and β7 containing Tyr194; U-loop, loop formed by residues 9−20 in the substrate-free structure; rmsd, root-mean-square deviation; K_M^{SAM} and K_M^{Gly}, apparent K_M values of SAM and Gly, respectively.

10.1021/bi034245a CCC: $25.00
Published on Web 06/24/2003

transferases (e.g., 0.4 μM for tRNA methyltransferases) (*5*). Thus, at physiological levels of SAM (0.1−0.2 μmol/g of liver) and SAH (0.02−0.06 μmol/g of liver), GNMT would exhibit appreciable activity. Therefore, fluctuation of GNMT activity would alter the SAM/SAH ratio, thereby influencing the activities of various methyltransferases.

Mudd et al. reported recently that a novel form of persistent isolated hypermethioninemia found in two Italian siblings was due to a deficiency of GNMT in the liver (*8*, *9*). May et al. found that the activity of hepatic GNMT increases and the activity of tRNA methyltransferase decreases in aging animals (*10*). Consequently, the concentrations of SAH and homocysteine are increased. Recent evidence indicates that chronic hyperhomocysteinemia, which is found in from 9% to 15% of the general population, is an independent risk factor for the development of atherosclerosis (*11*−*17*). Seshadri et al. suggested that an increased plasma homocysteine level is a strong, independent risk factor for the development of dementia and Alzheimer's disease (*18*). These results suggest that the activity of GNMT might contribute to atherosclerosis and Alzheimer's disease.

Fujioka et al. have characterized several important catalytic properties of GNMT. GNMT, unlike most SAM-dependent methyltransferases, is a homotetramer (*19*). GNMT binds its substrates in an obligatory order, with SAM as the first substrate (*20*). GNMT shows sigmoidal rate behavior with respect to SAM, but it shows no cooperativity toward Gly (*2*, *19*). The sigmoidal behavior is due to the equilibrium cooperative binding of SAM to the catalytic site residing on each subunit (i.e., a rapid and reversible binding of SAM occurs before the rate-limiting step), and the rate of breakdown of each enzyme−substrate complex is not affected by the presence or absence of ligands in other protomers (*21*). In the presence of SAM, cleavage of the eight residues of the N-terminus with trypsin occurred much more rapidly than in its absence (*21*).

The first crystal structure of GNMT revealed that GNMT is a dimer of dimers, in which the two subunits form a dimer by exchanging their N-termini (*22*). Each subunit has a unique "molecular basket" structure. A SAM-like molecule was trapped inside the basket, and the N-terminal U-loop of the partner subunit of the dimer blocked the basket. The SAM binding scheme was not consistent with those found in the other methyltransferases, suggesting that SAM sits on the minor binding site (*23*). The crystal structures of substrate-free GNMT and a mutated R175K enzyme have been determined (*23*, *24*). Those structures were isomorphous to that of the initial GNMT:SAM complex, except for the empty basket. The structure of R175K:SAH revealed that the enzyme has another conformation (*23*). The N-terminal U-loop of the partner subunit moves out, and a SAH molecule sits on the site occupied by the U-loop. The SAH binding mode is now consistent with those of the other methyltransferases. On the basis of crystal structures of the substrate-free GNMT and R175K:SAH, we have proposed that the N-terminus of GNMT regulates the enzyme activity (*23*). Before the catalysis, the N-terminal section of the partner subunit of the dimer competes with SAM to bind to the active site, and after the catalytic reaction, the same N-terminal section forces the departure of the potentially potent inhibitor SAH from the active site and thus facilitates the methyltransfer reaction.

Although the binding scheme of the adenosine moiety of SAH was relatively well-defined in the R175K:SAH structure, those of the homocysteine moiety of SAH and the second substrate Gly were not characterized due to the disordered structure of the N-terminal section (residues 1−43). Thus, it has been impossible to build a detailed catalytic mechanism of GNMT. Now, we have determined two new crystal structures of the ternary complex GNMT:(SAM + acetate) and the binary complex R175K:SAM and characterized the binding schemes of SAM and Gly. Here we report a detailed catalytic mechanism of GNMT based on the new crystal structures, and we have tested the proposed mechanism by a site-directed mutagenesis study.

EXPERIMENTAL PROCEDURES

Crystallization. WT and mutated enzymes were purified from *Escherichia coli* JM109 harboring the pCW-GNMT plasmids encoding the WT or mutated sequences (*25*). The hanging drop method of vapor diffusion was employed for crystallization of the enzymes. Thick plate-shaped crystals of GNMT:(SAM + acetate) and R175K:SAM suitable for X-ray diffraction studies were grown in a solution containing 5 mM SAM, 100 mM sodium citrate buffer (pH 5.6), 100 mM ammonium acetate, 50 mM NaCl, and 10% (w/v) PEG 3400 with a protein concentration of 20 mg/mL at 23 °C.

Data Measurement. A crystal (~0.3 × 0.3 × 0.1 mm) in a hanging drop was scooped by a nylon loop and was dipped into a cryoprotectant solution containing 20% ethylene glycol, 50 mM NaCl, 100 mM sodium citrate (pH 5.6), and 10% (w/v) PEG 3400 for 10 s before the crystal was frozen in cold nitrogen gas (−180 °C) on a Rigaku RAXIS imaging plate X-ray diffractometer with a rotating anode X-ray generator as an X-ray source (Cu Kα radiation operated at 50 KV and 100 mA). The X-ray beam was focused to 0.3 mm by confocal optics (Osmic, Inc.). The diffraction data were measured up to 2.8 Å resolution at −180 °C. The data were processed with the program DENZO/SCALEPACK (*26*). The data statistics are given in Table 1. The deduced unit cell dimensions indicate that the R175K:SAM crystal is isomorphous to the R175K:SAH crystal (*23*). On the other hand, the GNMT:(SAM + acetate) crystal is not isomorphous to either the R175K:SAM crystal or the substrate-free GNMT crystal.

Crystal Structure Determination of GNMT:(SAM + Acetate). The unit cell dimensions and space group indicated that an asymmetric unit contained one tetrameric enzyme. The crystal structure was determined by a molecular replacement procedure using AMORE (*27*). A subunit in the R175K:SAH complex structure, in which amino acid residues 1−44 were not defined, was used as the search model. The structure was refined with the POSITIONAL protocol and then the simulated annealing procedure of X-PLOR (*28*). The model of amino acid residues 18−44 was built in ($2F_o - F_c$) maps. ($F_o - F_c$) maps did not give any significant electron density for amino acid residues 1−17, indicating that these residues were heavily disordered. ($F_o - F_c$) maps showed two large significant residual electron density peaks in the region of the active site. Since GNMT was crystallized in the presence of an excess of SAM (5 mM) and acetate (100 mM), SAM and acetate molecules were fitted into the electron density peaks, respectively. Other well-defined residual electron

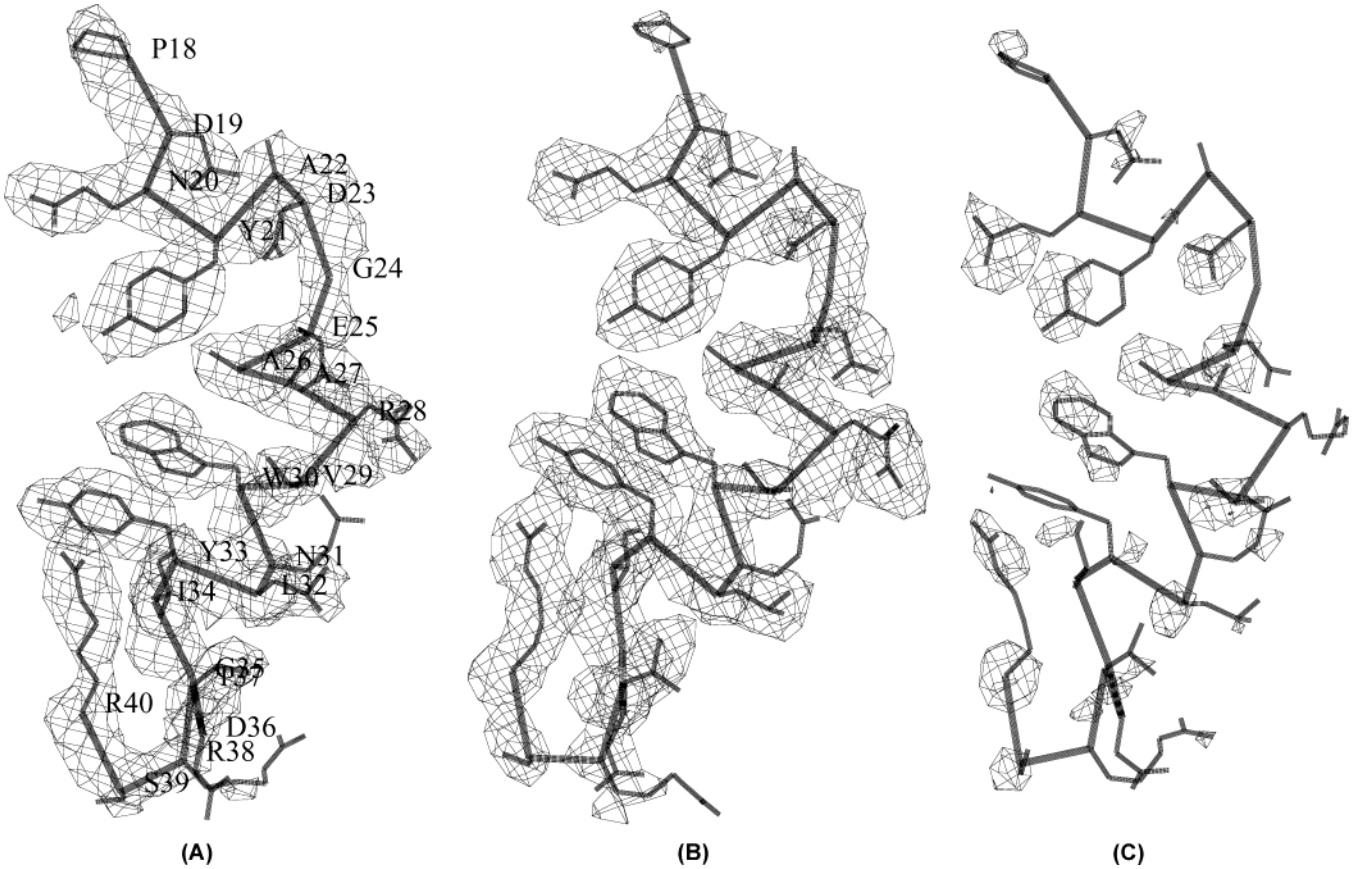

FIGURE 1: ($2F_o - F_c$) maps showing the electron density peaks of the N-terminus (amino acid residues 18−40). The contour is drawn at the 1.2σ level. Panels: (A) GNMT:(SAM + acetate) complex, (B) dimer AB in the R175K:SAM complex, and (C) dimer CD in the R175K:SAM complex.

density peaks in ($F_o - F_c$) maps were assigned to water molecules if peaks were able to bind the protein molecules with hydrogen bonds. The final model was refined by the simulated annealing procedure and followed by the individual *B*-factor refinement procedure of X-PLOR using bond and angle restraints. During the refinement, the four subunits related by a noncrystallographic 222 symmetry were tightly restrained to have the same structure in order to increase the accuracy of coordinates. To examine effects of the included water molecules to the crystal structure, the final structure was refined without water molecules by the same simulated annealing procedure for five times. The *R*- and free *R*-values increased from 0.204 to 0.226 and from 0.278 to 0.290, respectively. The rmsd between the protein atomic coordinates of the structures containing 290 water molecules and excluding all water molecules was less than 0.23 Å. Specifically, the rmsd of the amino acid residues involved in hydrogen bonds with the bound SAM and acetate molecules was less than 0.04 Å, suggesting that introducing 290 water molecules in the refinement would not change the geometry of the active site.

Crystal Structure Determination of R175K:SAM. The unit cell dimensions and the space group indicated that the crystal of R175K:SAM was isomorphous to the crystal of R175K:SAH (*23*). The structures were refined using 3.0 Å resolution data. A ($2F_o - F_c$) map showed significant electron density peaks for amino acid residues 19−44 in one dimer (AB) whereas there was no such electron density peaks in the other dimer (CD) (Figure 1). In the refinement procedure, two subunits in each dimer were restrained to have the same structure. ($F_o - F_c$) maps showed a large significant residual electron density peak in the region of the active site, and a SAM molecule was fitted into the electron density peak. The structure was refined with the same procedures applied to the GNMT:(SAM + acetate) complex. No water molecule was included in refinement.

Site-Directed Mutagenesis. Oligonucleotide-directed mutagenesis was used to prepare cDNAs encoding mutated forms of GNMT. Mutagenic oligonucleotides were purchased from Integrated DNA Technologies (Coraville, IA). Mutagenesis was performed by the method of Kunkel et al. (*29*), with a Mutan-K site-directed mutagenesis kit (Takara Shuzo, Kyoto, Japan). A clone containing the desired mutation was identified by nucleotide sequence analysis across the mutation site by the dideoxy chain termination method (*30*).

Enzyme Assay. The GNMT catalytic activities of the WT and mutated enzymes were determined spectrophotometrically. The assay mixture contained, in 2 mL of 50 mM potassium phosphate (pH 7.2), 60 μg of recombinant *S*-adenosyl-L-homocysteine hydrolase and 1.4 units of calf intestine adenosine deaminase (Sigma, St. Louis, MO). For the SAM kinetic parameter (V_{max} and K_M^{SAM}) measurement, five different concentrations of SAM (0.02−0.10 mM) with Gly concentration fixed were added to the reaction mixture. The Gly concentrations for the WT, Y21F, Y33F, Y194F, Y220F, and Y242F experiments were 5, 5, 250, 100, 250, and 5 mM, respectively. Similarly, for the Gly kinetic parameter (V_{max} and K_M^{Gly}) measurement, five different

Table 1: Experimental Details and Refinement Parameters of Crystal Structure Analyses[a]

crystal	GNMT: (SAM + acetate)	R175K:SAM
unit cell (Å)	90.95, 117.01, 137.78	77.87, 77.87, 227.11
space group	$P2_12_12_1$	$P4_3$
resolution (Å)	10−2.8	10.0−3.0
no. of reflections measured	195411	145578
no. of unique reflections[b]	36870	25540
% complete (outer shell)[c]	99 (97)	98 (96)
R_{sym}[d] (outer shell)	0.072 (0.258)	0.077 (0.266)
no. of protein atoms in asymmetric unit	8644	8214
no. of SAM and acetate in asymmetric unit	4 and 4	4 and 0
no. of water molecules in asymmetric unit	290	0
$I/\sigma(I)$ in outer shell[e]	2.9	3.1
R and free R	0.204 and 0.278	0.172 and 0.290
rms deviations		
bond (Å)	0.009	0.007
angle (deg)	1.49	1.25
torsion angle (deg)	23.8	27.6
mean B values		
C_α atoms (Å^2)	21.0	31.4
main chain (Å^2)	22.5	32.6
all atoms (Å^2)	23.8	33.8
Ramachandran plot		
most favored region (%)	89.5	91.4
additionally allowed region	10.1	8.1
allowed region	0.4	0.5

[a] M_r of subunit = 32400 (292 residues). [b] Unique reflections in the range between 10.0 Å and highest resolution. [c] Outer shell = 2.8−2.9 Å resolution for GNMT:(SAM + acetate) and 3.0−3.1 Å resolution for R175K:SAM. [d] $R_{sym} = \sum|I - \langle I\rangle|/\sum I$. [e] $I/\sigma(I)$ in the outer shell.

Table 2: Apparent Kinetic Parameters of WT and Mutated Enzymes

enzyme	k_{cat} (min^{-1})	SAM K_M (μM)	SAM k_{cat}/K_M[a]	Gly K_M (mM)	Gly k_{cat}/K_M[a]
WT	27(1)[b]	36(3)	1.00	0.43(4)	1.00
Y21F	6.3(3)	42(4)	0.20	0.24(2)	0.42
Y33F	12.7(8)	17(2)	0.99	25(2)	8.1×10^{-3}
Y194F	10.7(7)	35(3)	0.41	2.8(3)	6.1×10^{-2}
Y220F	10.7(8)	14(2)	1.02	30(3)	5.6×10^{-3}
Y242F	28(1)	32(4)	1.14	0.44(4)	0.99
R175K[c]	9.9(7)	35(3)	0.38	364(33)	4.3×10^{-4}

[a] Relative to the wild-type enzyme. [b] The standard errors of the last digits are given in parentheses. [c] From ref *23*.

concentrations of Gly with excess SAM (0.12 mM) were added to the reaction mixture. Due to a high UV absorption of SAM at 265 nm, the SAM concentration was kept to 0.12 mM. The reaction was started by adding the WT or mutated enzyme, and the decrease in absorbance at 265 nm due to the conversion of adenosine to inosine was followed at 30 °C. The product concentrations were calculated from the slope of ΔA and $\Delta\epsilon = 8.1 \times 10^3$ M^{-1}·cm^{-1} (*31*). The K_M and V_{max} values were determined from the Lineweaver−Burk plot using the least-squares regression method. The k_{cat} values listed in Table 2 were obtained by varying the SAM concentration at a fixed Gly concentration. It is noted that the N-terminus of the recombinant enzyme is not acetylated and the enzyme obeys Michalis−Menten kinetics at neutral pH (*25*, *32*).

RESULTS

Overall Crystal Structures. The crystallographic refinement parameters (Table 1), final ($2F_o - F_c$) maps, and conformational analysis by PROCHECK (*33*) indicate that the crystal structures of GNMT:(SAM + acetate) and R175K:SAM have been determined successfully. Except for the N-terminal section (amino acid residues 1−54), the topologies of all subunits in the GNMT structures are all the same and are ~β1(59−62)~α3(69−76)~β2(80−85)~α4-(88−100)~α4′(105−108)~β3(111−114)~α5(120−123)~β4-(130−135)~α6(151−161)~β5(164−175)~α7(177−183)~β6(199−209)~β7(212−223)~β8(235−242)~α8(247−257)~β9(262−267)~β10(283−290)~. The tertiary and quaternary structures of GNMT found in GNMT:(SAM + acetate) and R175K:SAM are quite similar to that of the substrate-free GNMT structure (*23*, *24*), except for the structures of the N-terminus, the Y194-loop between α7 and β6, and the active sites. The two subunits A and B interact with each other relatively strongly and form a dimer. Similarly, C and D form a dimer as well. The dimer structures of the substrate-free GNMT, R175K:SAM binary complex, and GNMT:(SAM + acetate) ternary complex are shown in Figure 2.

GNMT:(SAM + Acetate) Complex Structure. The four independent subunits related by a noncrystallographic 222 symmetry have the same structure. The rmsd among the four subunits is less than 0.045 Å. The N-terminal 1−17 amino acid residues in each subunit are apparently in the solvent region and are disordered. Amino acid residues 18−54 are ordered, in which residues 18−24 form a coil and residues 25−54 fold into a curved irregular α-helix A (Figure 2C). As expected, SAM molecules bind to the SAH binding site as seen in the R175K:SAH structure (*23*). The adenine ring is recognized by hydrogen bonds (N_1···N[Trp117], N_6···O_{D1}-[Asn116]) and the stacking interaction with indole ring of Trp117 (Figures 3 and 4). The consensus hydrogen bonds connect the 2′-OH and 3′-OH of adenosine ribose to acidic amino acid residue Asp85 located at the tip of β2. The carboxylate and amino groups of the Met moiety of SAM are involved in hydrogen bonding with Trp30, Arg40, Ala64, and Leu136. The O_H of Tyr21 is positioned to have a charge−dipole interaction (namely, $^{\delta-}$O···S$^+$ = 3.2 Å) with the positively charged S_D of SAM. An acetate is in the "Gly pocket" near the bound SAM. The carboxylate group of the bound acetate molecule forms a pair of hydrogen bonds with the guanidino group of Arg175. Tyr33, Tyr220, and Asn138 also participate in hydrogen bonds with the bound acetate. Distances and angles of possible hydrogen bonds are given in Table 3.

Model Structure of GNMT:(SAM + Gly). Since there was a space to fit an amino group above the C_A of acetate in the GNMT:(SAM + acetate) structure, a Gly molecule was built in the GNMT:(SAM + acetate) structure by the following procedures: the bound acetate was replaced with a Gly by attaching an amino group on the C_A of acetate, and the C−C_A bond was rotated until the N···C_E[SAM] distance became the minimum. In this model, the OH of Tyr194, the O of Gly137, and the C_E of SAM surround the N in a trigonal fashion (Figure 3). The distances of N···O_H, N···O, and N···C_E are 2.9, 2.9, and 2.7 Å, respectively, and the N is on the S_D−C_E vector. On the basis of this geometry, the lone

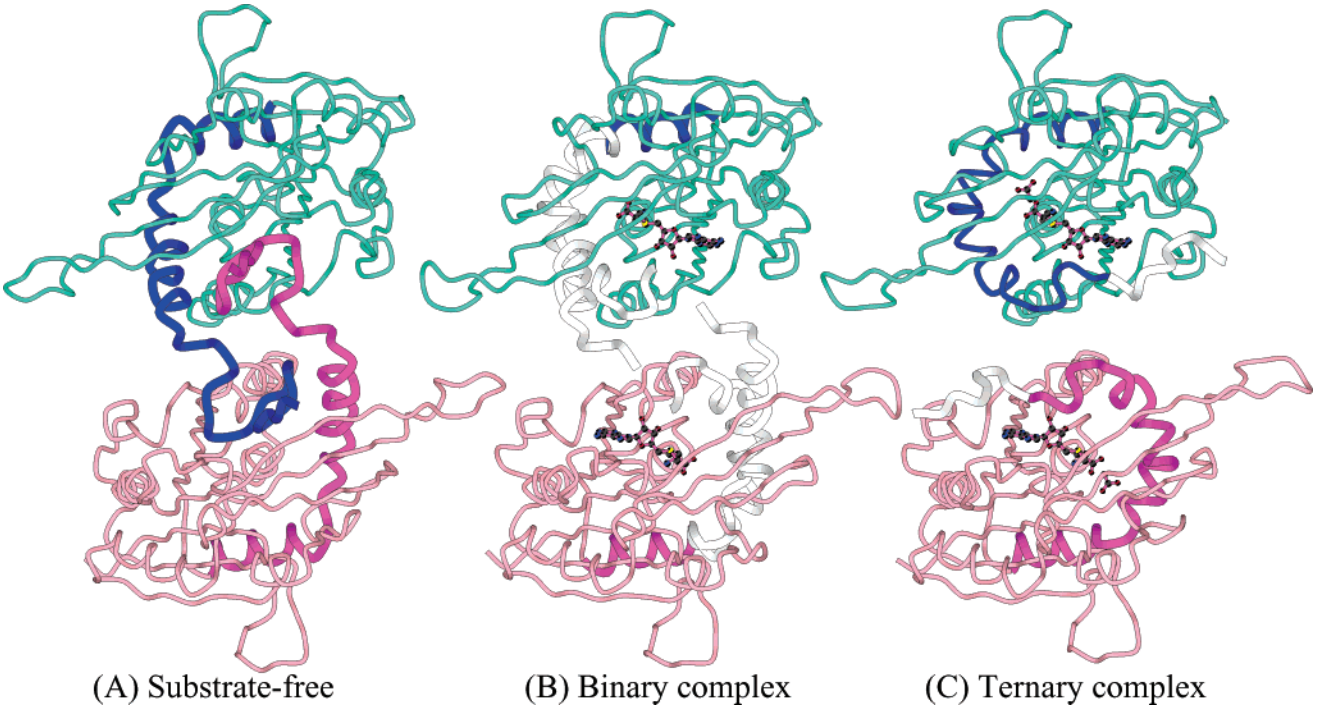

FIGURE 2: Three dimer structures showing the different N-terminal conformations. The two subunits are colored aquamarine and light pink. The N-terminal sections (amino acid residues 1−54) of each subunit are drawn with thick coils in blue and magenta, respectively. The disordered sections are indicated by white coils. The bound SAM and acetate molecules are illustrated with ball and stick presentation. Panels: (A) structure found in substrate-free GNMT, (B) structures found in R175K:SAH and dimer CD of R175K:SAM, and (C) structures found in GNMT:(SAM + acetate) and dimer AB of R175K:SAM.

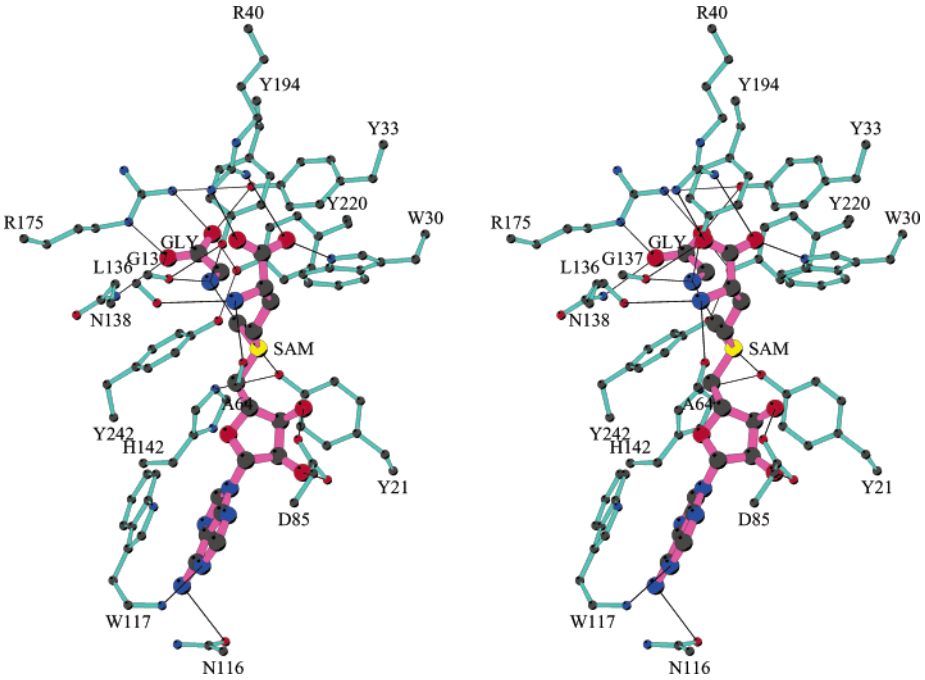

FIGURE 3: SAM and acetate in the active site of GNMT:(SAM + acetate). The Gly molecule is modeled by attaching an amino group to C_A of the bound acetate. SAM and Gly molecules are colored magenta while the protein sections are colored aquamarine. Thin lines illustrate possible hydrogen bonds between the substrates and protein.

pair orbital on the N of Gly should be pointed toward the C_E of SAM if the amino group is neutral (i.e., $-NH_2$). This GNMT:(SAM + Gly) model suggests that a S_N2 methyltransfer reaction can occur if the $N\cdots C_E$ distance is further shortened by a molecular vibration.

R175K:SAM Complex Structure. The R175K:SAM structure is isomorphous to the R175K:SAH structure (*23*). Although the R175K:SAM structure has a 222 symmetry, the two dimers (AB and CD) have slightly different structures. Dimer AB is similar to those of the GNMT:(SAM + acetate), and the N-terminal 1−18 amino acid residues are not visible (Figure 1B). Dimer CD is similar to that of R175K:SAH, and the N-terminal 1−43 amino acid residues are disordered (Figure 1C). Amino acid residues 18−43 apparently alternately form two conformations observed in the substrate-free GNMT and the GNMT:(SAM + acetate)

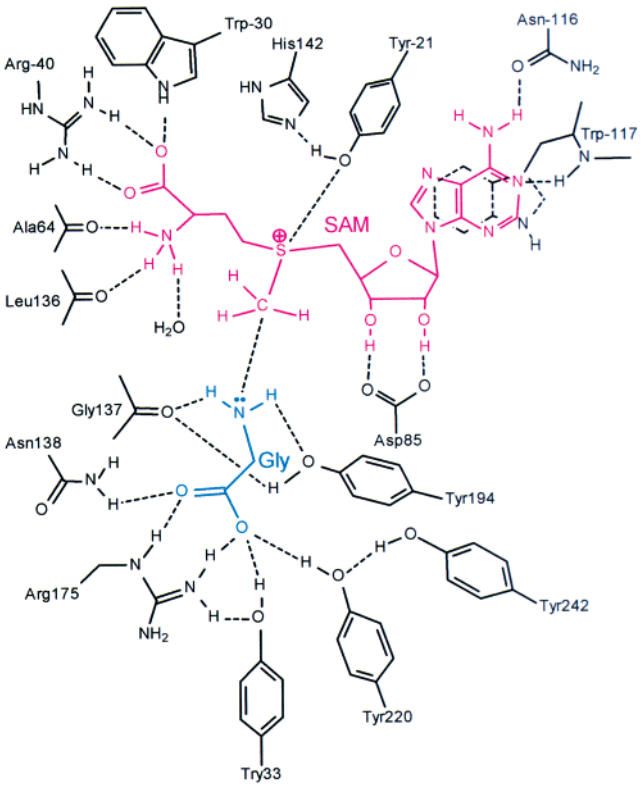

FIGURE 4: Schematic diagram showing the interaction of SAM and Gly in the active site. Broken lines indicate the possible hydrogen bonds (Table 3). S_D of SAM and O_H of Tyr21 separated by 3.2 Å and C_E of SAM and N of Gly separated by 2.7 Å are connected by a broken line. It is noted that Tyr21, Trp30, Tyr33, and Arg40 are disordered in R175K:SAH and in dimer CD of R175K:SAM and, thus, are not involved in the hydrogen bonds with SAM. Also, Ala64 and Leu136 do not participate in hydrogen bonds with SAM in those dimer structures.

complex (Figure 5). The rmsd between the subunits within the dimer are 0.065 Å for dimer AB and 0.057 Å for dimer CD, whereas the rmsd between the two dimers is 0.974 Å, indicating that the two dimers are significantly different. In dimer AB, the bound SAM has the same hydrogen-bonding scheme and the stacking interactions with the SAM in the GNMT:(SAM + acetate) structure. A Gly pocket is formed near the bound SAM, but there is no Gly/acetate since R175K does not have the Gly binding Arg175. In dimer CD, although the adenosine moiety of the SAM has the same interactions as observed in the dimer AB, the Met moiety does not form any hydrogen bonds with the amino acid residues Tyr21, Trp30, and Arg40, which are now disordered. The presence of two different dimers in the R175K:SAM complex structure suggests that absence of Gly/acetate increases mobility of the helix A.

Enzyme Activity. Apparent kinetic parameters of Y21F, Y33F, Y194F, Y220F, and Y242F mutated enzymes are given in Table 2. There is no significant reduction of the catalytic rates (k_{cat}) by the mutations. None of the mutation changes significantly the value of K_M^{SAM}. Only the Y33F and Y220F mutations increased significantly the K_M^{Gly} values and reduced significantly their catalytic efficiencies (k_{cat}/K_M^{Gly}). The k_{cat}/K_M^{SAM} of Y21F and k_{cat}/K_M^{Gly} of Y194F suggest that these mutations reduce slightly the catalytic efficiencies. The Y242F mutation had no effect on catalysis.

Table 3: Distances (Å) and Angles (deg) of Possible Hydrogen Bonds[a]

hydrogen bond A−X(H)···Y−B	distance (Å) X(H)···Y	angle (deg) A−X(H)···Y	angle (deg) X(H)···Y−B
[Y21]C_Z−O_H···N_{E2}−C_{E1}[H142]	2.87(2)	130(1)	85(1)
[W30]C_{E2}−N_{E1}···O_2−C[SAM]	2.89(4)	134(1)	132(1)
[Y33]C_Z−O_H···O_2−C[Gly]	2.57(5)	127(1)	147(1)
[R40]C_Z−N_{H1}···O_2−C[SAM]	3.27(3)	116(1)	86(1)
[R40]C_Z−N_{H2}···O_1−C[SAM]	2.61(5)	99(1)	145(2)
[W117]C_A−N···N_1−C_2[SAM]	2.87(2)	132(1)	117(1)
[N138]C_G−N_{D2}···O_1−C[Gly]	2.78(3)	121(1)	154(1)
[R175]C_D−N_E···O_1−C[Gly]	2.85(2)	123(1)	118(1)
[R175]C_Z−N_{H2}···O_2−C[Gly]	2.67(1)	127(1)	112(1)
[R175]C_Z−N_{H2}···O_H−CZ[Y33]	3.45(2)	171(1)	172(2)
[Y194]C_Z−O_H···O_1−C[G137]	2.75(1)	135(1)	123(1)
[Y220]C_Z−O_H···O_2−C[Gly]	2.67(3)	114(1)	102(1)
[Y242]C_Z−O_H···O_H−CZ[Y220]	2.61(2)	121(1)	138(1)
[SAM]C_6−N_6···O_{D1}−CG[N116]	2.86(2)	116(1)	88(1)
[SAM]$C_{2'}$−$O_{2'}$···O_{D2}−CG[D85]	2.57(1)	138(1)	109(1)
[SAM]$C_{3'}$−$O_{3'}$···O_{D1}−CG[D85]	3.03(3)	109(1)	123(1)
[SAM]C_A−N···O−C[A64]	3.18(3)	115(1)	161(1)
[SAM]C_A−N···O−C[L136]	3.36(3)	146(1)	132(1)
[SAM]C_A−N···O_{H2}[H_2O]	3.00(20)	110(3)	
[Gly]C_A−N···O−C[G137][b]	2.89(3)	152(1)	168(2)
[Gly]C_A−N···O_H−C_Z[Y194][b]	2.89(2)	117(2)	105(1)
[Y21]C_Z−O_H···S_D−C_E[SAM][c]	3.21(2)	112(1)	77(1)
[SAM]S_D−C_E···N−C_A[Gly][b,d]	2.66(2)	176(1)	128(1)

[a] The mean values of the four subunits are listed along with the rmsd values in parentheses. It is noted that the crystallographic estimated standard deviations would be larger than the rmsd values. The bound Gly is built as follows: the amino group (N) was attached to C_A of the bound acetate, and the C−C_A bond was rotated until the N···C_E[SAM] distance became the minimum. [b] Values are from the GNMT:(SAM + Gly) model structure (see footnote *a*). [c] Charge−dipole interaction. [d] Short C_E···N distance between SAM and Gly.

DISCUSSION

Crystal structures of the substrate-free GNMT (*23*, *24*) and its R175K mutated enzyme (*23*), R175K:SAH (*23*), R175K:SAM (this study), and GNMT:(SAM + acetate) (this study) have been determined. These structures show the various stages of the catalytic process of GNMT. An analysis of these structures reveals why GNMT behaves differently from the other SAM-dependent methyltransferases and can regulate the SAM/SAH ratio in cells; i.e., GNMT has a much larger K_M^{SAM} value than other SAM-dependent methyltransferases and is only weakly inhibited by SAH. As described below, the GNMT catalysis is quite dynamical.

The types of catalytic mechanisms that enzymes employ have been grouped into six classes: acid−base catalysis, covalent catalysis, metal ion catalysis, electrostatic catalysis, proximity and orientation effects, and preferential binding of the transition state complex. On the basis of the GNMT:(SAM + acetate) crystal structure and the GNMT:(SAM + Gly) model structure, we propose that GNMT catalyzes the methyltransfer reaction by "proximity and orientation effects".

A Proposed Catalytic Mechanism of GNMT. (A) Initial Stage. The structure of substrate-free GNMT represents this stage (Figure 2A). The U-loop section (residues 9−20) of the N-terminus of the partner subunit of the dimer enters the active site and occupies the SAM binding site (closed conformation). The edge section of the U-loop (residues 21−24) is apparently flexible so that the U-loop of the partner subunit readily moves out of the active site. At low SAM concentrations, the U-loop and SAM compete to bind the

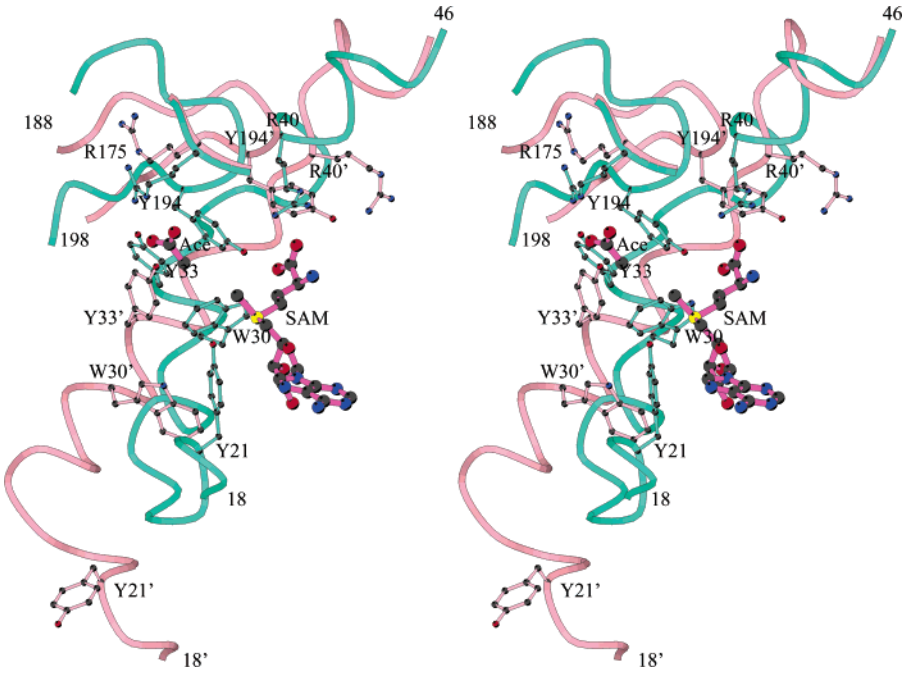

FIGURE 5: Superimposed view of the N-terminal sections (amino acid residues 18−46) of the substrate-free GNMT (light pink) and the GNMT:(SAM + acetate) complex (aquamarine). The backbones from amino acid residues 18−46 are illustrated by coils. The side chains participating in the SAM and acetate bindings are illustrated by a ball and stick presentation. SAM and acetate in the GNMT:(SAM + acetate) complex are shown by magenta. Arg175, the Gly binding site, is illustrated in order to show a swing movement of the side chain. The substrate-free GNMT structure was superimposed on the GNMT:(SAM + acetate) complex structure by spatially aligning the catalytic domains (amino acid residues 55−176 and 246−292) using a least-squares method. For the Y194 loop, the skinny loop and fat loop seen in the substrate-free GNMT and dimer AB of R175K:SAM are shown, respectively.

active site, with the equilibrium toward the closed conformation. Therefore, GNMT shows a relatively high K_M^{SAM} in comparison with the other methyltransferases.

(B) SAM Binding Stage. The structure of dimer CD in R175K:SAM represents this stage (Figure 2B). As the SAM concentration is increased, the equilibrium between the closed conformation and the open conformation (U-loop is moved out and SAM occupies the site) shifts toward SAM binding. At the initial binding, the SAM connects its adenosine moiety to Asp85, Asn116, and Trp117 by hydrogen-bonding and $\pi-\pi$ interactions, but its Met moiety has little interaction with the protein. The section of residues 25−54 forms alternately two conformations [L-shaped helix(25−35)−coil-(36−40)−helix(41−54) and curved irregular α-helix A] (Figure 5). When it forms the helix A conformation, the following events occur. The N-terminal end of helix A fills the space occupied by the U-loop of the partner subunit, and thus, the SAM entrance to the active site is closed. The helix A forms three hydrogen bonds with the bound SAM and two hydrogen bonds with another part of the protein ([Tyr21]-$O_H\cdots N_{E2}$[His142]; [Tyr33]$O_H\cdots N_{H2}$[Arg175]). The Met moiety of SAM is now very tightly connected to the enzyme by five hydrogen bonds (Figure 4). Furthermore, the S_D has a charge−dipole interaction with the O_H of Tyr21.

(C) Gly Binding Stage. The structure of dimer AB in R175K:SAM represents this stage (Figure 2C). The conformation change in the section of residues 25−54 allows Arg40 to push Tyr194 into the active site and creates a Gly pocket near the bound SAM. The pushing of Tyr194 also changes the conformation of the Y194-loop from a "skinny loop" to a "fat loop" (Figure 5). A Gly enters through the fat loop, and its negatively charged carboxylate group binds to the positively charged guanidino group of Arg175 by forming a pair of hydrogen bonds. This pair of hydrogen bonds orients the Gly toward the Gly pocket. The bound Gly on the side chain of Arg175 is quite far from the bound SAM, and the side chain is apparently able to swing since there is no hydrogen bond partner around the guanidino group (Figure 5). The bound Gly on the swinging side chain of Arg175 is fitted into the Gly pocket and is connected by five additional hydrogen bonds to the protein. Also the guanidino group of Arg175 is connected to Tyr33 (Figures 3 and 4). Now, the bound Gly molecule is also very tightly connected to the protein by seven hydrogen bonds.

(D) Near the Transition State. The crystal structure of GNMT:(SAM + acetate) represents this stage (Figure 2C). The conformation change in the N-terminal section (residues 1−54) brings a SAM and a Gly into the active site in the correct order, connects the two substrates firmly to the protein, stabilizes the positive charge on the S_D of SAM, and aligns the lone pair orbital of the amino nitrogen (N) of Gly to the methyl carbon (C_E) of SAM. Five hydrogen bonds ($O_{T1}\cdots N_{D2}$[Asn138]; $O_{T2}\cdots O_H$[Tyr33]; N$\cdots O_H$[Tyr194], N$\cdots$O[Gly137], [Arg175]$N_{H1}\cdots O_H$[Tyr33]) connect the Gly in the proximity of the bound SAM. Thermal motion of the enzyme leads to a collision of the N and C_E so that a S_N2 methyltransfer reaction occurs. The $S_D\cdots O_H$[Tyr21] charge−dipole interaction facilitates the S_N2 reaction (Figure 6).

(E) Product Releasing Stage. The crystal structure of R175K:SAH represents this stage (Figure 2B). Once the methyltransfer reaction is completed, the transferred bulky methyl group destabilizes the hydrogen bonds around the N, and eventually these hydrogen bonds are broken. Furthermore, the positive charge on N destabilizes the charge−charge interaction between the negatively charged carboxylate group of sarcosine and the positively charged guanidino

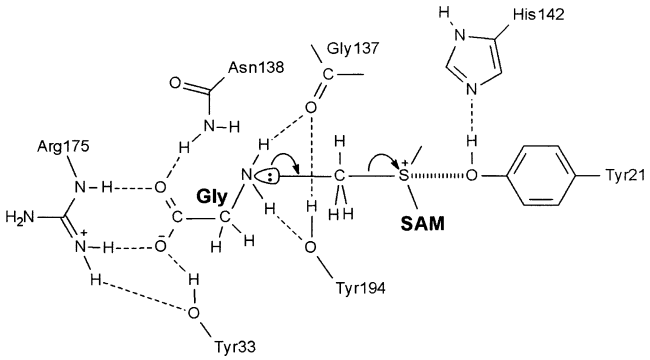

FIGURE 6: Schematic diagram of the proposed methyltransfer reaction of GNMT. The amino nitrogen (N) of Gly is on the C_E-S_D vector and its lone pair orbital is precisely pointed to the methyl carbon (C_E) of SAM. The positively charged S_D of SAM has a charge−dipole interaction with the O_H of Tyr21. The five hydrogen bonds ($O_{T1}\cdots N_{D2}$[Asn138]; $O_{T2}\cdots O_H$[Tyr33]; $N\cdots O_H$[Tyr194], N···O[Gly137], [Arg175]$N_{H1}\cdots O_H$[Tyr33]) connect the Gly in the proximity of the bound SAM and orient the lone pair orbital on the amino nitrogen (N) of Gly toward the donor methyl group (C_E) of SAM. Under these conditions, the S_D-C_E bonding electron is pulled toward the positively charged S_D, and the lone pair electrons on the N interact with the C_E. Thermal motion of the enzyme leads to a collision of the N and C_E so that a S_N2 methyltransfer reaction occurs. The charge−dipole interaction $S_D\cdots O_H$[Tyr21] facilitates the reaction.

group of Arg175. Therefore, the product sarcosine is readily released from the active site. After the methyl transfer, the S_D of SAH becomes neutral, so that the $S_D\cdots O_H$[Tyr21] charge−dipole interaction vanishes, and helix A increases its mobility. Subsequently, the hydrogen bonds between the substrates and the helix A are broken, and helix A goes back to the initial conformation (i.e., an L-shaped helix−coil−helix conformation). Arg40 pushes Tyr194 away from the active site, and the Y194 loop changes to the initial conformation. The association of SAH is weakened because the hydrogen bonds between the homocysteine moiety of SAH and the protein are broken.

(F) Final Stage. The series of the conformational changes in the partner subunit bring its U-loop to the front of the active site, and then the U-loop competes with the product SAH to bind the active site. Eventually, the equilibrium shifts toward the closed conformation; i.e., the weakly associated SAH leaves the active site, and the U-loop occupies the SAM/SAH binding site (Figure 2A). Therefore, GNMT is weakly inhibited by SAH in comparison with the other methyltransferases.

Kinetic Data Support the Proximity and Orientation Effects Catalysis of GNMT. Since the substitution of Tyr residue with Phe residue does not cause any steric hindrance in the protein structure, structures of the mutated proteins are expected not to have changed. There are five Tyr residues (21, 33, 194, 220, 242) on the active site surface. Tyr21 interacts weakly with the S_D of SAM, Tyr33 and Tyr220 form hydrogen bonds with the carboxyl group of Gly and firmly attach it to the enzyme, and Tyr194 along with the carbonyl oxygen of Gly137 is expected to orient the lone pair electrons on the N to the S_D of SAM. The Y33F and Y220F mutations are expected to increase the K_M^{Gly} values, and Y21F and Y194F mutations are expected to reduce slightly their catalytic efficiency k_{cat}/K_M. As listed in Table 2, the Y33F and Y220F mutations increase significantly the K_M^{Gly} values, and the Y194F mutation produces a marginal increase in the K_M^{Gly} value. The catalytic efficiencies are significantly reduced by the Y33F and Y220F mutations, and marginal reductions are seen in the Y21F and Y194F mutations. Although Tyr242 locates near the active site, the Y242F mutation does not change the kinetic parameters, indicating that Tyr242 is indeed not directly involved in the catalysis.

From the substrate-free GNMT and the GNMT:(SAM + acetate) structures, the side chain of Arg175 moves substantially (Figure 5). Apparently, the roles of Arg175 are to provide a Gly binding site and to bring the bound Gly into the Gly pocket. Therefore, the R175K mutation is considered to affect the catalysis much more severely in comparison with the Y21F, Y33F, Y194F, and Y220F mutations. In the R175K:SAM and R175K:SAH structures, there is no acetate molecule binding to the N_Z of Lys175, suggesting that a free Gly has to enter the Gly pocket by itself in the case of the R175K mutated enzyme. For this reason, the K_M^{Gly} value is much higher than those of the Y21F, Y33F, Y194F, and Y220F mutated enzymes.

In conclusion, the kinetics data of mutated enzymes support the proposed catalytic mechanism of GNMT.

Defect GNMTs in Italian Siblings. The mutations found in two Italian siblings are L49P and H175N, which correspond to L48P and H174N mutations in the rat enzyme (*8*, *9*). Since Leu48 is located in the regular α-helical section of helix A and Pro is a helix breaker, the L48P mutation changes the conformation of helix A. Consequently, the L48P mutated enzyme could lose catalytic activity. In the case of the H174N mutation, His174 is situated on strand β5 and next to the Gly binding residue, Arg175, which is located on the C-terminal end of strand β5. The H174N mutation apparently changes the side-chain orientation of Arg175. Consequently, the Gly-bound Arg175 cannot fit into the Gly pocket as described above. The details of the H174N mutation will be discussed elsewhere along with D173N and N176A mutations.

ACKNOWLEDGMENT

We express our thanks to Professor Richard H. Himes and Richard L. Schowen for a critical reading of the manuscript and for very valuable comments.

NOTE ADDED AFTER PRINT PUBLICATION

The Protein Data Bank code (1NBH) was incorrect in the version published on the Web 06/24/03 (ASAP) and in the July 22, 2003, issue (Vol. 42, No. 28, pages 8394−8402). The correct electronic version of the paper was published 8/19/03, and an Addition and Correction appears in the September 16, 2003, issue (Vol. 42, No. 36).

REFERENCES

1. Blumenstein, J., and Williams, G. R. (1960) The enzymic *N*-methylation of glycine, *Biochem. Biophys. Res. Commun. 3*, 259−263.
2. Ogawa, H., Gomi, T., and Fujioka, M. (1993) Mammalian glycine *N*-methyltransferases. Comparative kinetic and structural properties of the enzymes from human, rat, rabbit and pig livers, *Comp. Biochem. Physiol. 106B*, 601−611.
3. Kerr, S. J. (1972) Competing methyltransferase systems, *J. Biol. Chem. 247*, 4248−4255.

4. Yeo, E.-J., and Wagner, C. (1994) Tissue distribution of glycine *N*-methyltransferase, a major folate binding protein of liver, *Proc. Natl. Acad. Sci. U.S.A. 91*, 210−214.
5. Kerr, S. J., and Heady, J. E. (1974) Modulation of tRNA methyltransferase activity by competing enzyme systems, *Adv. Enzyme Regul. 12*, 103−117.
6. Cantoni, G. L., Richards, H. H., and Chiang, P. K. (1978) Inhibitors of *S*-adenosylhomocysteine hydrolase and their role in the regulation of biological methylation, in *Transmethylation* (Usdin, E., Borchardt, R. T., and Creveling, C. R., Eds.) pp 155−164, Elsevier/North Holland, New York.
7. Wittwer, A. J., and Wagner, C. (1981) Identification of the folate-binding proteins of rat liver mitochondria as dimethylglycine dehydrogenase and sarcosine dehydrogenase. Purification and folate-binding characteristics, *J. Biol. Chem. 256*, 4102−4108.
8. Luka, Z., Cerone, R., Phillips, J. A., III, Mudd, H. S., and Wagner, C. (2002) Mutations in human glycine *N*-methyltransferase give insights into its role in methionine metabolism, *Hum. Genet. 110*, 68−74.
9. Mudd, S. H., Cerone, R., Schiaffino, M. C., Fantasia, A. R., Minniti, G., Caruso, U., Lorini, R., Watkins, D., Matiaszuk, N., Rosenblatt, D. S., Schwahn, B., Rozen, R., LeGros, L., Kotb, M., Capdevila, A., Luka, Z., Finkelstein, J. D., Tangerman, A., Stabler, S. P., Allen, R. H., and Wagner, C. (2001) Glycine *N*-methyltransferase deficiency: a novel inborn error causing persistent isolated hypermethioninaemia, *J. Inherit. Metab. Dis. 24*, 448−464.
10. Mays, L. L., Borek, E., and Finch, C. E. (1973) Glycine *N*-methyltransferase is a regulatory enzyme which increases in aging animals, *Nature 243*, 411−413.
11. Brattstrom, L., and Wilcken, D. E. (2000) Homocysteine and cardiovascular disease: cause or effect?, *Am. J. Clin. Nutr. 72*, 315−323.
12. Ueland, P. M., Refsum, H., Beresford, S. A., and Vollset, S. E. (2000) The controversy over homocysteine and cardiovascular risk, *Am. J. Clin. Nutr. 72*, 324−332.
13. Reeder, S. J., Hoffmann, R. L., Magdic, K. S., and Rodgers, J. M. (2000) Homocysteine: the latest risk factor for heart disease, *Dimens. Crit. Care Nurs. 19*, 22−28.
14. Miller, J. W. (2000) Homocysteine, Alzheimer's disease, and cognitive function, *Nutrition 16*, 675−677.
15. Finkelstein, J. D. (2000) Homocysteine: a history in progress, *Nutr. Rev. 58*, 193−204.
16. McKinley, M. C. (2000) Nutritional aspects and possible pathological mechanisms of hyperhomocysteinaemia: an independent risk factor for vascular disease, *Proc. Nutr. Soc. 59*, 221−237.
17. Perry, I. J. (1999) Homocysteine and risk of stroke, *J. Cardiovasc. Risk 6*, 235−240.
18. Seshadri, S., Beiser, A., Selhub, J., Jacques, P. F., Rosenberg, I. H., D'Agostino, R. B., Wilson, P. W., and Wolf, P. A. (2002) Plasma homocysteine as a risk factor for dementia and Alzheimer's disease, *N. Engl. J. Med. 346*, 476−483.
19. Ogawa, H., and Fujioka, M. (1982) Purification and properties of glycine *N*-methyltransferase from rat liver, *J. Biol. Chem. 257*, 3447−3452.
20. Konishi, K., and Fujioka, M. (1987) Chemical modification of a functional arginine residue of rat liver glycine methyltransferase, *Biochemistry 26*, 8496−8502.
21. Konishi, K., and Fujioka, M. (1988) Rat liver glycine methyltransferase, Cooperative binding of *S*-adenosylmethionine and loss of cooperativity by removal of short NH_2-terminal segment, *J. Biol. Chem. 263*, 13381−13385.
22. Fu, Z., Hu, Y., Konishi, K., Takata, Y., Ogawa, H., Gomi, T., Fujioka, M., and Takusagawa, F. (1996) Crystal structure of glycine *N*-methyltransferase from rat liver, *Biochemistry 35*, 11985−11993.
23. Huang, Y., Komoto, J., Konishi, K., Takata, Y., Ogawa, H., Gomi, T., Fujioka, M., and Takusagawa, F. (2000) Mechanisms for auto-inhibition and forced product release in glycine *N*-methyltransferase: crystal structures of wild-type, mutant R175K and *S*-adenosylhomocysteine-bound R175K enzymes, *J. Mol. Biol. 298*, 149−162.
24. Pattanayek, P., Newcomer, M. E., and Wagner, C. (1998) Crystal structure of apo-glycine *N*-methyltransferase (GNMT), *Protein Sci. 7*, 1326−1331.
25. Ogawa, H., Gomi, T., Takata, Y., Date, T., and Fujioka, M. (1997) Recombinant expression of rat glycine *N*-methyltransferase and evidence for contribution of N-terminal acetylation to co-operative binding of *S*-adenosylmethionine, *Biochem. J. 327*, 407−412.
26. Otwinowski, Z., and Minor, W. (1997) Processing of X-ray diffraction data collected in oscillation mode, *Methods Enzymol. 276*, 307−326.
27. Navaza, J. (1994) AMoRe: An Automated Package for Molecular Replacement, *Acta Crystallogr. D50*, 157−163.
28. Brünger, A. T. (1993) X-PLOR 3.82: A system for X-ray crystallography and NMR, Yale University Press, New Haven and London.
29. Kunkel, T. A., Roberts, J. D., and Zakour, R. A. (1987) Rapid and efficient site-specific mutagenesis without phenotypic selection, *Methods Enzymol. 154*, 367−382.
30. Sanger, F., Nicklen, S., and Coulson, A. R. (1977) DNA sequencing with chain-terminating inhibitors, *Proc. Natl. Acad. Sci. U.S.A. 74*, 5463−5467.
31. Takata, Y., Konishi, K., Gomi, T., and Fujioka. M. (1994) Rat guanidinoacetate methyltransferase. Effect of site-directed alteration of an aspartic acid residue that is conserved across most mammalian *S*-adenosylmethionine-dependent methyltransferases, *J. Biol. Chem. 269*, 5537−5542.
32. Ogawa, H., Konishi, K., Takata, Y., Nakashima, H., and Fujioka, M. (1987) Rat glycine methyltransferase: Complete amino acid sequence deduced from a cDNA clone and characterization of the genomic DNA, *Eur. J. Biochem. 168*, 141−151.
33. Laskowski, R. A., MacArthur, M. W., Moss, D. S., and Thornton, J. M. (1993) PROCHECK: A program to check the stereochemical quality of protein structures, *J. Appl. Crystallogr. 26*, 283−291.

BI034245A